Broadband Dielectric Function of Nonequilibrium Warm Dense Gold

Y. Ping,[1] D. Hanson,[2] I. Koslow,[2] T. Ogitsu,[1] D. Prendergast,[1] E. Schwegler,[1] G. Collins,[1] and A. Ng[1,2]

[1]*Lawrence Livermore National Laboratory, Livermore, California, USA*

[2]*Department of Physics & Astronomy, University of British Columbia, Vancouver, British Columbia, Canada*

(Received 15 May 2006; published 26 June 2006)

We report on the first single-state measurement of the broadband (450–800 nm) dielectric function of gold isochorically heated by a femtosecond laser pulse to energy densities of $10^6 - 10^7$ J/kg. A Drude and an interband component are clearly seen in the imaginary part of the dielectric function. The Drude component increases with energy density while the interband component shows both enhancement and redshift. This is in strong disagreement with predictions of a recent calculation of dielectric function based on limited Brillouin zone sampling.

DOI: 10.1103/PhysRevLett.96.255003 PACS numbers: 52.50.Jm, 52.25.Fi, 52.25.Os, 52.38.−r

Warm dense matter refers to states characterized by comparable thermal and Fermi energies, and ion-ion coupling parameters [1] that exceed unity. While theoretical treatment of warm dense matter is made difficult by effects of electron degeneracy, excited states, and strong ion-ion coupling, experimental study is made challenging by the need to obtain single-state data as theory benchmarks. This has left warm dense matter a largely uncharted frontier. Nonetheless, warm dense matter is drawing increasing attention because of its role in understanding the convergence between condensed matter and plasma physics, as well as its relevance to other areas including shock physics [2], inertial confinement fusion [3], and astrophysics [4]. Among this broad interest, a new focus is nonequilibrium warm dense matter. This is driven by its practical importance as transient states in laboratory-produced high energy density matter and its fundamental significance in the study of relaxation processes and phase transitions.

A key parameter characterizing warm dense matter is its dielectric function, $\varepsilon(\omega)$. Encompassing contributions from intraband and interband transitions, it is central to the understanding of electron transport and optical properties. In addition, it is a manifestation of band structure and density of state effects, thus rendering it a plausible means of probing structural phases. This is of intense interest to the study of warm dense matter produced not only by laser excitation but also by shock compression. Changes in the imaginary part of the spectral dielectric function in low energy density states have been studied extensively in thermomodulation spectroscopy [5–12] including reflectivity and transmissivity measurements. The only available single-state data on the dielectric properties of highly nonequilibrium warm dense matter are the dc and ac conductivities of gold heated by a femtosecond laser to energy densities of 10^5–10^7 J/kg [13]. However, the latter is measured at a single photon energy of 1.55 eV (wavelength of 800 nm) and is thus the result of intraband transitions. On the other hand, *ab initio* calculation of the dielectric function of aluminum across the solid-liquid transition has been obtained [14]. Most recently, ac conductivity of warm dense gold in a spectral range that covers both intraband and interband transitions has been reported, albeit based on very limited Brillouin zone sampling [15].

In this Letter we present the first measurement of broadband (450–800 nm) dielectric function of highly nonequilibrium warm dense gold using a pump-probe technique (femtosecond laser pump and supercontinuum probe [16]). It yields the first single-state data at high energy densities with simultaneous observations of intraband and interband components with sub-ps resolution. The results verify Drude-like behavior at 800 nm. They also reveal an enhancement and redshift of the *d-p* band transitions that persist until the heated sample disassembles. The measured data provide a critical benchmark for theory and point to the importance of adequate Brillouin zone sampling to ensure convergence in calculations.

The experiment is performed using two synchronized pulses from a Ti:sapphire laser (the Europa Laser at LLNL). A 150 fs FWHM, 400 nm pulse is used to produce isochoric heating of a freestanding gold nanofoil (25–33 nm thick) while a 180 fs FWHM, 800 nm pulse is focused onto a CaF_2 crystal to generate a supercontinuum probe [17] for broadband optical measurements. The gold nanofoil is mounted over an aperture of 600 μm diameter. The flatness of its central 300 μm diameter is better than $\lambda/10$ as determined with a 632.8 nm Michelson interferometer. The 400 nm pump pulse is focused onto the nanofoil at normal incidence with a spot diameter of 80 μm (FWHM). The incident, reflected and transmitted light are monitored by both calibrated photodiodes and CCD cameras to yield measurements of laser deposition across the focal spot with a spatial resolution of 5 μm. While the skin-depth of 400 nm light is only $\sim$7 nm in gold, the electron ballistic range is $\sim$110 nm [18] that far exceeds the thickness of the target. Combined with the 150 fs pulse width, this results in uniform and isochoric heating of the nanofoil at solid density and allows the determination of excitation energy density $\Delta\epsilon$ directly from the laser deposition measurement.

The supercontinuum probe illuminates the gold nanofoil at a 45° incidence with a 30 μm $\times$ 600 μm line focus, covering both heated and unheated regions of the target.

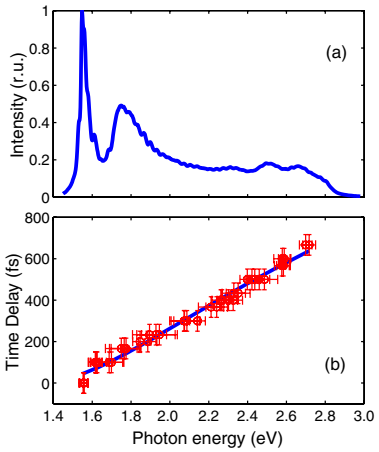

FIG. 1 (color online). (a) Supercontinuum spectrum and (b) frequency chip in the supercontinuum probe.

Figure 1(a) shows a measured supercontinuum spectrum. The frequency chirp in the supercontinuum source [Fig. 1(b)] is measured using the Kerr optical-gate technique [19]. To remove the effect of chirp in measurements, spectral data are binned in 10 nm intervals and appropriate temporal shifts are applied using Fig. 1(b). The reflected and transmitted spectra of the supercontinuum probe are recorded with two intensified CCD cameras. Spatially and frequency resolved reflectivity R^* and transmissivity T^* in the heated region are determined using *in situ* calibration from the unheated region of the target. These are used to solve the Helmholtz equations for a gradient-free dielectric slab in accordance with the idealized slab plasma concept [20] to yield both the real part, $\varepsilon_1(\omega)$, and the imaginary part, $\varepsilon_2(\omega)$, of the dielectric function.

Figs. 2(a) and 2(b) show the temporal evolution of $\varepsilon(\omega)$ of gold at an excitation energy density of $(2.9 \pm 0.3) \times 10^6$ J/kg. The data have been corrected for frequency chirp as described above. Time zero corresponds to the onset of changes in R^* and T^* from their room-temperature values. This is found to be the same for all frequencies in the supercontinuum spectrum after chirp correction. Also included in the figure are tabulated data of gold at room temperature [21]. The minimum energy required for d-p transitions is ~2.3 eV. In an earlier study at an excitation energy density of 4.0×10^6 J/kg [22] it was found that the dielectric function at 1.55 eV showed an initial transient consisting of a decrease (increase) in the real (imaginary) part to a minimum (maximum) value in ~600 fs. This was followed by an increase (decrease) to a quasi-steady-state value in ~900 fs. The quasi-steady state then lasted for another ~4 ps before apparent target disassembly occurred. The time steps in Fig. 2 are chosen to span a similar duration. The new data at 1.55 eV show similar transient and quasi-steady-state behaviors as described above. A single $\varepsilon(\omega)$ plot is presented for 1.2–4.0 ps since no significant change in $\varepsilon(\omega)$ is observed in the interval,

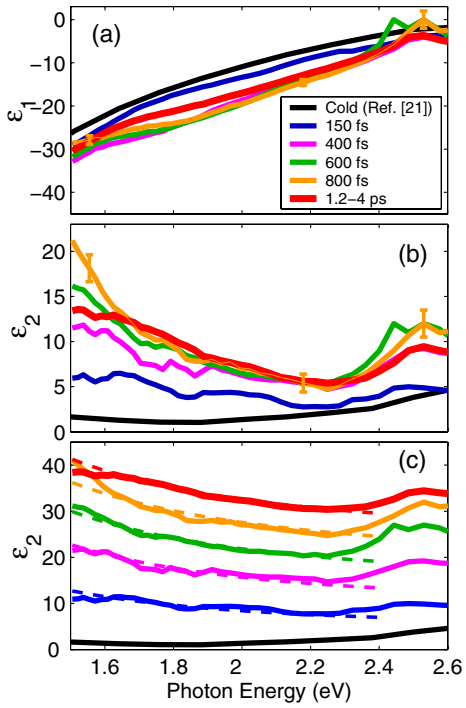

FIG. 2 (color online). (a) $\varepsilon_1(\omega)$ and (b) $\varepsilon_2(\omega)$ at different times for an energy density of 2.9×10^6 J/kg, and (c) $\varepsilon_2(\omega)$ displayed with an offset of +5 along the y axis between time steps. Sample error bars are included in (a) and (b).

consistent with the quasi-steady state found in a previous study [22].

For the observed spectral range, $\varepsilon_1(\omega)$ appears relatively featureless. However, intraband and interband (d-p) components are clearly discernable in $\varepsilon_2(\omega)$ below and above ~2.3 eV. They also show substantial enhancements over their room-temperature values. Furthermore, by displaying $\varepsilon_2(\omega)$ at different time steps with an offset [Fig. 2(c)], it can readily be seen that the intraband component shows good agreement with best-fitted Drude functions [23] that assume frequency-independent electron collision time and density, except possibly for a small region around 1.6 eV at the peak of the transient at 800 fs. The fitting parameters are given in Table I.

TABLE I. Parameters for Drude fitting in Figs. 2 and 3.

	$\Delta\epsilon$ (10^6 J/kg)	Probe Delay	τ (10^{-15} s)	n_e (10^{22} cm^{-3})
(a)	2.90	150 fs	1.49	4.54
(b)	2.90	400 fs	1.16	6.01
(c)	2.90	600 fs	0.97	6.34
(d)	2.90	800 fs	0.87	6.45
(e)	2.90	1.2–4.0 ps	0.83	5.93
(f)	2.20	1.4–2.0 ps	1.00	5.10
(g)	4.70	1.4–2.0 ps	0.86	7.00
(h)	17.0	1.4–2.0 ps	0.77	8.40

To examine the dependence of $\varepsilon(\omega)$ on the excitation energy density $\Delta\epsilon$, we use measurements made on the quasi-steady state. The results are presented in Fig. 3. These are not corrected for frequency chirp and the probe delay varies from 1.4 ps at 1.55 eV to 2.0 ps at 2.6 eV. Time zero again corresponds to the onset of observed changes in R^*, T^* at 1.55 eV. For $\Delta\epsilon$ of 2.2×10^6 and 4.7×10^6 J/kg, the 1.4–2.0 ps probe delay falls completely within the quasi-steady state duration [22] allowing the dielectric function to be determined over the entire spectral range of 1.5–2.7 eV. However, at 1.7×10^7 J/kg no solution to the Helmholtz equations can be found for $\varepsilon(\omega)$ from the R^*, T^* data above 2.38 eV. This is due to the breakdown of the uniform slab assumption as target disassembly gives rise to gradients in the expanding foil. The cutoff point at 2.38 eV corresponds to a probe delay of 1.9 ps that is consistent with the disassembly time observed in the earlier experiment [22]. Accordingly, dielectric function measurement using a frequency chirped source offers a new means of probing hydrodynamic disassembly of a heated solid.

With increasing excitation energy density, the quasi-steady state $\varepsilon_1(\omega)$ begins to reveal the effect of interband (d-p) transitions above 2.1 eV while $\varepsilon_2(\omega)$ exhibits increasing enhancements in intraband and interband transitions. The intraband component continues to be Drude-like as indicated by the best-fitted Drude functions in the figure. The fitting parameters are also given in Table I. It should be noted that the quasi-steady state collision time and electron density are in good agreement with previous measurements [13]. The interband component also shows a redshift that increases with excitation energy density.

Ab initio calculations of the ac conductivity of warm dense states of gold have been reported recently by Mazevet *et al.* [15]. Their results show a highly structured frequency spectrum with a local maximum between 1.7–1.9 eV and the absence of any well-defined redshift or enhancement of the interband component above 2 eV. This deviates substantially from our observation described above. To understand the cause for the discrepancy, we calculate $\varepsilon_2(\omega)$ based on density functional theory within local density approximation [24]. Our focus is on the convergence of the calculation in terms of finite-size effect on the electronic degrees of freedom, *i.e.*, on sampling of the Brillouin zone. We approximate the ionic cores of the gold atoms using Troullier-Martins pseudopotentials [25] and we expand the electron wave functions in a plane wave basis using a kinetic energy cutoff of 40 Ry. All calculations are limited to the fcc primitive cell and the lattice constant is kept fixed at the bulk value of 4.052 Å, since earlier measurements indicate the absence of significant expansion during the quasi-steady state of the gold foil [13,22]. $\varepsilon_2(\omega)$ is then calculated using the Kubo-Greenwood formula [26], where only interband contributions are considered and a frozen core is adopted to approximate the all-electron valence wave functions in our estimation of the necessary velocity matrix elements [27].

A crucial aspect of such an *ab initio* approach is the choice of the k-point mesh used to sample the Brillouin zone. This can greatly impact the accuracy in calculating interband contributions to the dielectric function [14], especially in the case of gold, where the characteristic transition peaks originate from a small area in the Brillouin zone where branches of the bands involved become parallel. In our calculation of $\varepsilon_2(\omega)$ for a perfect fcc gold crystal at 0 K, convergence is reached using a uniform grid of 128^3 k points, as shown in Fig. 4. Our estimate of $\varepsilon_2(\omega)$ is in excellent agreement with that obtained from an all-electron localized basis-set approach [28]. This indicates that for a 32-atom gold system, sampling over 65 000 k points is required to ensure fidelity of the calculation. It is evident from Fig. 4 that insufficient Brillouin zone sampling can readily generate substantial fluctuations in the dielectric function. This may account for the highly struc-

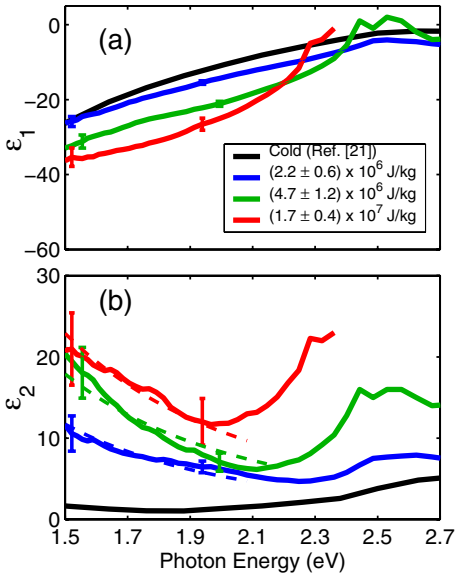

FIG. 3 (color online). (a) $\varepsilon_1(\omega)$ and (b) $\varepsilon_2(\omega)$ for different excitation energy densities. Sample error bars are included.

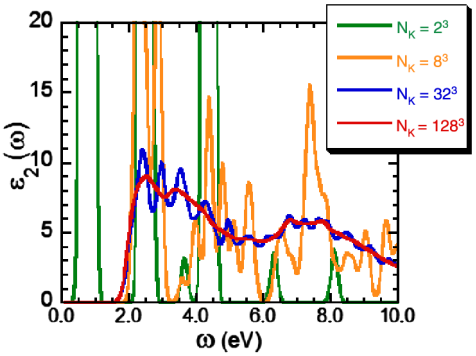

FIG. 4 (color online). $\varepsilon_2(\omega)$ of gold at 0 K calculated with different Brillouin zone sampling. N_k is the number of k points.

tured conductivities seen in previous calculations of a 32-atom system with sampling over only 4 k points [15], which roughly corresponds to 8^3 k points with a fcc unit cell. It may contribute to the spurious local maximum seen at 1.7–1.9 eV giving it a non-Drude appearance.

In conclusion, our new measurements have given us some interesting insights to the behavior of ultrafast laser excited gold. A basic property contained in the spectral dielectric function is electron density of state. Thus, the data in Fig. 2 carry information on the evolution of the density of the d and s/p states driven by the processes of photo-excitation of d electrons, electron-hole recombination, and electron-electron thermalization at high energy densities. Similarly, the data in Fig. 3 carry information on the dependence of density of state on excitation energy density. For the range of conditions of interest, Drude-like behavior of the intraband component of $\varepsilon_2(\omega)$ is confirmed. This provides a crucial validation for the use of ac conductivity at 800 nm to derive dc conductivity, collision time and carrier density of warm dense gold [13], thus significantly enhancing the utility of ac conductivity measurement. The appearance of interband transitions presents the first evidence of the persistence of d band in the quasi-steady state of ultrafast laser heated gold. If it can be assumed that the presence of a d band can only result from long-range ordering, this raises the possibility that the quasi-steady state is the characteristic of a superheated solid which would be consistent with a recent empirical two-temperature model [15]. Equally important are the observed increases in redshift and enhancement of d-p transitions with excitation energy density. Redshifts in the interband transition region may result from temperature-induced changes in the energy distribution of the electrons. The enhancement is, however, unexpected. Calculations of optical absorption spectrum of equilibrium solid and liquid phases of aluminum [14] show only redshifts in interband transitions but no enhancements as the solid is heated to its melting point, consistent with observation [29]. On the other hand, measurements of electron energy distribution function of ultrafast laser excited gold [30] have shown that even at very low excitation energy densities (300 μJ/cm^2 or equivalently $\sim 5 \times 10^5$ J/kg for a 30 nm thick gold foil), a small energetic electron tail appears to remain visible 670 fs after the laser pump pulse. We are thus led to conjecture that our observed enhancements in d-p transitions are likely the manifestation of nonequilibrium density of state resulting from the complex processes of electron-hole recombination and electron-electron relaxation in states driven to very high energy densities.

In addition, our data have provided the first benchmark for testing theory [15]. We believe that insufficient Brillouin zone sampling is the likely cause for the noted discrepancy between theory and experiment. This points to the need for examining proper convergence of numerical calculations with regard to finite-size effects.

We wish to thank L. Bendict for valuable discussions. This work was performed under the auspices of the U.S. Department of Energy by University of California Lawrence Livermore National Laboratory under Contract No. W-7405-ENG-48 and was supported by the Natural Sciences and Engineering Research Council of Canada.

[1] S. Ichimaru, Rev. Mod. Phys. **54**, 1017 (1982).
[2] A. Ng *et al.*, Laser Part. Beams **23**, 527 (2005).
[3] T. R. Dittrich *et al.*, Phys. Plasmas **6**, 2164 (1999).
[4] D. Saumon *et al.*, High Press. Res. **16**, 331 (2000).
[5] W. J. Scouler, Phys. Rev. Lett. **18**, 445 (1967).
[6] R. Rosei and D. W. Lynch, Phys. Rev. B **5**, 3883 (1972).
[7] R. Rosei *et al.*, Surf. Sci. **37**, 689 (1973).
[8] R. Rosei, Phys. Rev. B **10**, 474 (1974).
[9] E. Colavita *et al.*., Phys. Rev. B **20**, 4864 (1979).
[10] J. E. Nestrell, Jr. *et al.*, Phys. Rev. B **21**, 3173 (1980).
[11] E. Colavita *et al.*, Phys. Rev. B **27**, 4684 (1983).
[12] H. E. Elsayed-Ali and T. Juhasz, Phys. Rev. B **47**, 13 599 (1993).
[13] K. Widmann *et al.*, Phys. Rev. Lett. **92**, 125002 (2004).
[14] L. X. Benedict, J. E. Klepeis, and F. H. Streitz, Phys. Rev. B **71**, 064103 (2005).
[15] S. Mazevet *et al.*, Phys. Rev. Lett. **95**, 085002 (2005).
[16] L. Huang, J. P. Callan, E. N. Glezer, and E. Mazur, Phys. Rev. Lett. **80**, 185 (1998).
[17] R. Huber, H. Satzger, W. Zinth, and J. Wachtveitl, Opt. Commun. **194**, 443 (2001).
[18] J. Hohlfeld *et al.*, Chem. Phys. **251**, 237 (2000).
[19] C. Nagura *et al.*, Appl. Opt. **41**, 3735 (2002).
[20] A. Forsman *et al.*, Phys. Rev. E **58**, R1248 (1998).
[21] P. B. Johnson and R. W. Christy, Phys. Rev. B **6**, 4370 (1972).
[22] T. Ao *et al.*, Phys. Rev. Lett. **96**, 055001 (2006).
[23] P. Drude, Ann. Phys. (Leipzig) **1**, 566 (1900).
[24] D. M. Ceperley and B. J. Alder, Phys. Rev. Lett. **45**, 566 (1980); J. P. Perdew and A. Zunger, Phys. Rev. B **23**, 5048 (1981).
[25] N. Troullier and J. L. Martins, Phys. Rev. B **43**, 1993 (1991).
[26] R. Kubo, J. Phys. Soc. Jpn. **12**, 570 (1943); D. A. Greenwood, Proc. Phys. Soc. London **A71**, 585 (1958).
[27] H. Kageshima and K. Shiraishi, Phys. Rev. B **56**, 14 985 (1997).
[28] P. Romaniello and P. L. de Boeij, J. Chem. Phys. **122**, 164303 (2005).
[29] A. G. Mathewson and H. P. Meyers, J. Phys. F **2**, 403 (1972).
[30] W. S. Fann *et al.*, Phys. Rev. B **46**, 13 592 (1992).